JEM

Article

Therapeutically targeting tumor microenvironment–mediated drug resistance in estrogen receptor–positive breast cancer

Kevin Shee,[1] Wei Yang,[1] John W. Hinds,[1] Riley A. Hampsch,[1] Frederick S. Varn,[1,3] Nicole A. Traphagen,[1] Kishan Patel,[1] Chao Cheng,[1,3] Nicole P. Jenkins,[2] Arminja N. Kettenbach,[2] Eugene Demidenko,[3] Philip Owens,[5,6] Anthony C. Faber,[7] Todd R. Golub,[8] Ravid Straussman,[9] and Todd W. Miller[1,4]

[1]Department of Molecular and Systems Biology and [2]Department of Biochemistry and Cell Biology, Norris Cotton Cancer Center, Geisel School of Medicine at Dartmouth, Lebanon, NH
[3]Department of Biomedical Data Science, Geisel School of Medicine at Dartmouth, Lebanon, NH
[4]Comprehensive Breast Program, Norris Cotton Cancer Center, Geisel School of Medicine at Dartmouth, Lebanon, NH
[5]Department of Cancer Biology, Vanderbilt University School of Medicine, Nashville, TN
[6]Research Medicine, Veterans Affairs, Tennessee Valley Healthcare System, Nashville, TN
[7]VCU Philips Institute for Oral Health Research, School of Dentistry and Massey Cancer Center, Virginia Commonwealth University, Richmond, VA
[8]Broad Institute of MIT and Harvard, Cambridge, MA
[9]Department of Molecular Cell Biology, Weizmann Institute of Science, Rehovot, Israel

Drug resistance to approved systemic therapies in estrogen receptor–positive (ER+) breast cancer remains common. We hypothesized that factors present in the human tumor microenvironment (TME) drive drug resistance. Screening of a library of recombinant secreted microenvironmental proteins revealed fibroblast growth factor 2 (FGF2) as a potent mediator of resistance to anti-estrogens, mTORC1 inhibition, and phosphatidylinositol 3-kinase inhibition in ER+ breast cancer. Phosphoproteomic analyses identified ERK1/2 as a major output of FGF2 signaling via FGF receptors (FGFRs), with consequent up-regulation of Cyclin D1 and down-regulation of Bim as mediators of drug resistance. FGF2-driven drug resistance in anti-estrogen–sensitive and –resistant models, including patient-derived xenografts, was reverted by neutralizing FGF2 or FGFRs. A transcriptomic signature of FGF2 signaling in primary tumors predicted shorter recurrence-free survival independently of age, grade, stage, and FGFR amplification status. These findings delineate FGF2 signaling as a ligand-based drug resistance mechanism and highlights an underdeveloped aspect of precision oncology: characterizing and treating patients according to their TME constitution.

INTRODUCTION

Breast cancer is the most commonly diagnosed malignancy among women, with an estimated 1.7 million new cases per year worldwide (Siegel et al., 2012; Ferlay et al., 2015). Despite advances in screening, therapeutics, and molecular understanding, this disease remains the leading cause of non–smoking-related cancer death (American Cancer Society, 2015). Approximately 60% of breast cancers express estrogen receptor (ER) α, which generally indicates a degree of estrogen dependence, without overexpressing the HER2/*ERBB2* proto-oncogene. Approved therapeutics for the treatment of ER-positive (ER+) breast cancer include anti-estrogens that target ER: selective ER modulators such as tamoxifen that directly antagonize ER, aromatase inhibitors that suppress estrogen production to block estrogen-dependent ER activity, and selective ER down-regulators such as fulvestrant (fulv) that directly antagonize ER and promote ER degradation. Anti-estrogen–resistant disease develops in one third of patients treated in the adjuvant setting and eventually occurs in nearly all patients with metastatic disease (Ferlay et al., 2010; Early Breast Cancer Trialists' Collaborative Group (EBCTCG) et al., 2011). One of the best-characterized mechanisms of anti-estrogen resistance is hyperactivation of the phosphatidylinositol 3-kinase (PI3K)–AKT–mTOR (mechanistic target of rapamycin) pathway (Miller et al., 2011). Such evidence drove the clinical development of agents such as the approved mTORC1 inhibitor (mTORC1i) everolimus and experimental PI3K inhibitors (PI3Ki) such as pictilisib (Krop et al., 2016) for use in combination with anti-estrogens. Despite initial clinical benefit from such combination therapies in the metastatic setting, most patients inevitably develop drug resistance, highlighting the need for identification and targeting of additional resistance mechanisms.

Correspondence to Todd W. Miller: todd.w.miller@dartmouth.edu

The Rockefeller University Press
J. Exp. Med. 2018 Vol. 215 No. 3 895–910
https://doi.org/10.1084/jem.20171818

Preclinical success in cancer drug development rarely translates into clinical success (Hay et al., 2014). This dichotomy between drug sensitivity of cancer cell lines and lack of efficacy in patient tumors suggests that the noncancer components of the tumor microenvironment (TME) may play important roles in modulating treatment outcomes. The TME consists of both cellular components (e.g., fibroblasts, endothelial cells, immune cells, and adipocytes) and noncellular components (e.g., extracellular matrix, cytokines, and oxygenation), both of which can promote tumor development and progression (Quail and Joyce, 2013). An early example of the importance of the TME in modulating response to therapeutics involved the demonstration that tumor cells resistant to alkylating agents in vivo became drug sensitive when cultured ex vivo (Teicher et al., 1990). Similarly, tumors grown subcutaneously versus orthotopically showed different responses to doxorubicin (Fidler et al., 1994). TME-mediated drug resistance has since been previously implicated in response to some targeted therapies, such as BRAF inhibitors in $BRAF^{V600E}$ mutant melanoma (Straussman et al., 2012; Wilson et al., 2012; Klemm and Joyce, 2015). However, the role of TME components in modulating therapeutic response in ER+ breast cancer is practically unknown. We hypothesized that secreted factors within the TME can uniquely modulate response to anti-estrogen therapy in ER+ breast cancer and used a novel microenvironmental secreted factor screening approach to comprehensively identify TME-targeted therapeutic opportunities in ER+ breast cancer.

RESULTS

Secreted cytokine screening reveals ligands that modulate response to anti-estrogens, PI3Ki, and mTORC1i in ER+ breast cancer

We designed a set of screens to determine whether secreted proteins in the TME confer resistance to anti-estrogens. A summary of the screening workflow is shown in Fig. 1 A. A discovery screen was performed with MCF-7 and T47D ER+ breast cancer cells, the anti-estrogen fulv, and 297 soluble recombinant proteins (e.g., cytokines and extracellular matrix) known to be part of the human secretome. Analysis revealed a candidate hit list of 14 secreted factors that rescued from fulv (z-score ≥ 1) and four factors that sensitized to fulv (z-score ≤ -1; Fig. 1 B).

A follow-up validation screen was performed with fulv and 24 secreted factors from the discovery screen (Table S1). We found a dose-dependent increase in fulv resistance or sensitization with individual factors (Fig. 1 C). The results of the discovery and validation screens were well correlated ($R^2 = 0.36$; $P = 0.002$), particularly when excluding five secreted factors that rescued in the discovery screen, but not the validation screen ($R^2 = 0.81$; $P < 0.0001$; Fig. S1 A).

A well-characterized mechanism of resistance to anti-estrogen therapy is activation of the PI3K–AKT–mTOR pathway (Miller et al., 2011), which led to the clinical development of PI3Ki and mTORi for ER+ breast cancer. To test the ability of cytokines to broadly modulate sensitivity to anti-estrogens (e.g., fulv, 4-hydroxytamoxifen), PI3Ki (e.g., pictilisib), and mTORC1i (e.g., everolimus), we performed an expansion screen with four cell lines (MCF-7, T47D, ZR75-1, and HCC-1500) and 13 validated cytokines (Fig. 1 D). Interestingly, many of the cytokines that modulated anti-estrogen sensitivity similarly modulated response to PI3Ki and mTORC1i in all four cell lines ($R^2 = 0.20$–0.61; all $P \leq 0.002$; Fig. S1 B).

Only a fraction of the secreted factors in our screen are likely to be applicable to the TMEs associated with ER+ breast cancer. To delineate which hits are most likely to be present in these TMEs, a bioinformatics scoring algorithm was developed using mRNA and protein expression profiles from normal tissues as surrogates for noncancerous cells in the TME. Available tissue mRNA and/or protein expression data for 14 rescue hits from the discovery screen were extracted from databases (GTEx Consortium, 2015; Uhlén et al., 2015) to compare levels in breast tissue components (breast mammary, adipose, and primary fibroblasts) and common metastatic sites of ER+ breast cancer (bone marrow, lung, and liver; Fig. S1, D and E). The discovery screen hit with the highest integrated mRNA and protein TME expression score was fibroblast growth factor 2 (FGF2; basic FGF; Figs. 1 E and S1 F). Notably, rescue by other FGF family ligands was not ubiquitous (Fig. S1 G), and most FGFs are not expressed in ER+ breast cancer–relevant tissues (GTEx Consortium, 2015; Uhlén et al., 2015). Furthermore, FGF2 is not highly expressed in ER+ breast cancer cell lines, especially when compared with expression in other cancer cell lines, ruling out autocrine signaling (Fig. S1, H–J). Although we confirmed that the HER3/ErbB3 ligand neuregulin 1 (NRG1) potently conferred drug resistance in ER+ breast cancer cells (Fig. 1 D; Larsen et al., 1999; Kodack et al., 2017), NRG1 was found to be absent or weakly expressed at the mRNA and protein levels in the ER+ breast cancer–relevant normal tissues represented in our TME algorithm (Fig. S1, D and E).

FGF2 activates FGF receptor (FGFR) signaling to suppress apoptosis, proliferative arrest, and drug sensitivity

Long-term growth assays confirmed that FGF2 mediated rescue from 4-hydroxytamoxifen, fulv, pictilisib, everolimus, and combinations of fulv/pictilisib and fulv/everolimus in MCF-7 and T47D cells (Figs. 2 A and S2 A). We found no such rescue from the DNA-damaging chemotherapeutic doxorubicin. To determine whether FGF2 rescue requires FGFR signaling, cells were treated with or without the FGF2-neutralizing mouse antibody GAL-F2 or the pan-FGFR kinase inhibitor PD-173074, and co-treated with or without FGF2 and drugs. Treatment with GAL-F2 or PD-173074 effectively abrogated FGF2-mediated rescue from anti-estrogens, PI3Ki, and mTORC1i (Fig. 2 A). FGF2 significantly abrogated fulv-, pictilisib-, and everolimus-induced G1 cell cycle arrest and apoptosis (Fig. 2, B and C), suggesting that FGF2 rescues from anticancer agents by driving cell proliferation and preventing

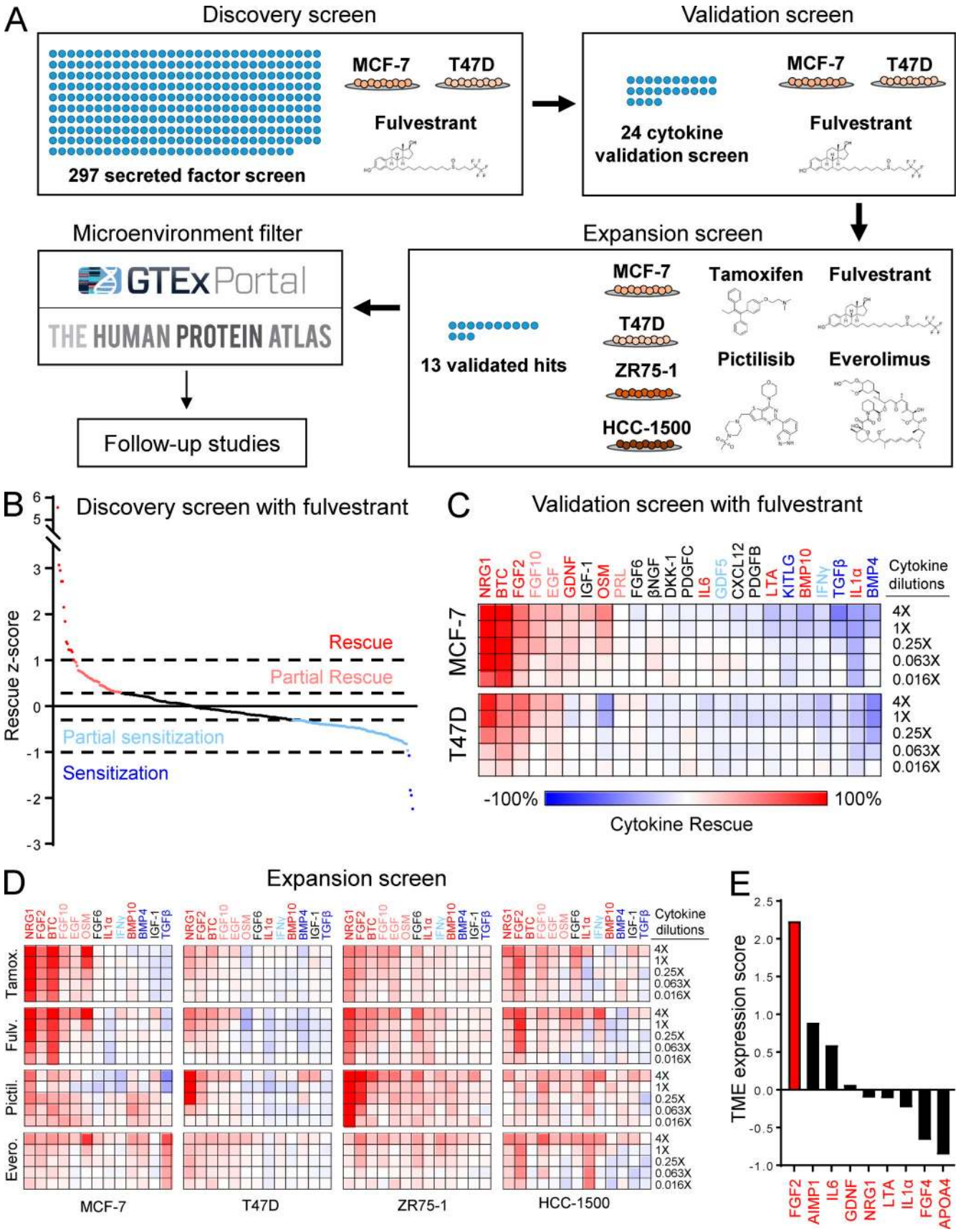

cell death. Drug target engagement was validated by immunoblot (Fig. S2, B and C).

FGF2/FGFR signaling activates MEK–ERK to drive Bim down-regulation and Cyclin D1 up-regulation

To efficiently and comprehensively identify signaling networks induced by FGF2 in ER+ breast cancer cells, phosphoproteomic profiling was performed using stable isotope labeling with amino acids in cell culture (SILAC)–based proteomics on three pairs of cell lysates: (1) MCF-7 ± FGF2, (2) MCF-7 + fulv ± FGF2, and (3) T47D + fulv ± FGF2. Analyses of peptides with increased phosphorylation (mean greater than or equal to twofold, $P \leq 0.05$) revealed significantly enriched FGF2-induced phosphorylation of ERK1 at Y204 and T202:Y204 and ERK2 at Y187 and T185 :Y187, both characteristic of canonical MAPK pathway signaling (Fig. 3 A and Table S2). Furthermore, analysis of all residues with increased phosphorylation (mean greater than or equal to twofold, $P \leq 0.05$) in the presence of FGF2 revealed significant enrichment of motifs known to be associated with ERK1/2 activation (Fig. S2 D). Immunoblot analysis revealed strong and consistent FGF2-induced, FGFR-dependent phosphorylation of ERK1/2, the upstream MAPK kinases 1 and 2 (MEK1/2), and FGFR substrate 2α (FRS2α), which is the primary adaptor involved in FGFR-induced MEK/ERK activation (Kouhara et al., 1997; Figs. 3 B and S2 C). Co-treatment with the MEK inhibitor trametinib suppressed FGF2-mediated rescue from 4-hydroxytamoxifen, fulv, and everolimus (Fig. S2 F).

MEK–ERK pathway activation can affect many downstream targets implicated in the cell cycle and survival (Caunt et al., 2015). We analyzed a large panel of apoptosis- and cell cycle–related proteins to delineate potential mechanisms underlying FGF2-mediated rescue from anticancer agents in ER+ breast cancer cells. FGF2 treatment consistently decreased levels of the proapoptotic protein Bim, which was up-regulated in the presence of anticancer agents (Figs. 3 C and S3 A); Bim is destabilized by phosphorylation by ERK1/2 (Hübner et al., 2008). FGF2 also up-regulated multiple cyclins, including Cyclin D1, which activates CDK4 and CDK6 as a key mediator of cell cycle progression in ER+ breast cancer (Figs. 3 C and S3 A; Yu et al., 2001). FGF2-induced Bim down-regulation, Cyclin D1 up-regulation, and Rb phosphorylation (a marker of CDK4/6 activity and G1 to S progression) were observed in all four cell lines (Figs. 3 C and S3 B). Co-treatment with trametinib suppressed FGF2-mediated Bim down-regulation and Cyclin D1 up-regulation, implicating MEK–ERK in responses to FGF2 (Fig. S3 C). We also tested whether other FGFs could similarly activate FRS2α and ERK, down-regulate Bim, and induce Cyclin D1 in ER+ breast cancer cells. The pattern of these pathway changes paralleled the ability of each FGF ligand to rescue cells from anti-estrogens, PI3Ki, and mTORC1i (Fig. S3 D).

To determine whether FGF2-mediated decreases in apoptosis are dependent on Bim down-regulation, we used RNAi. Bim knockdown suppressed apoptosis induced by fulv, pictilisib, or everolimus in anti-estrogen–sensitive cells and abrogated FGF2-mediated rescue (Fig. 3 D and Fig. S3, E and F). We also tested the requirement for Cyclin D1 in FGF2-induced cell cycle progression. Knockdown of Cyclin D1 promoted G1 arrest and abrogated FGF2-mediated decreases in cell cycle arrest (Figs. 3 E and S3 G). Furthermore, co-treatment with the CDK4/6 inhibitor palbociclib abrogated FGF2-mediated rescue from anti-estrogens, PI3Ki, and mTORC1i (Figs. 3 F and S3 H), suggesting that FGF2-mediated rescue involves Cyclin D1–CDK4/6 signaling.

FGF2 mediates resistance to PI3K- and mTORC1-directed combination therapies in anti-estrogen–resistant ER+ breast cancer

Because PI3Ki and mTORi inhibitors are being developed for the treatment of recurrent/metastatic ER+ breast cancer, where many patients have anti-estrogen refractory disease, the effects of FGF2, GAL-F2, and PD-173074 were tested in fulv-resistant (FR) MCF-7 (MCF-7/FR) and ZR75-1 (ZR75-1/FR) cells. FGF2 rescued MCF-7/FR cells from combinations of fulv/pictilisib and fulv/everolimus, but not from fulv/doxorubicin (Fig. 4 A). Treatment with GAL-F2 or PD-173074 effectively abrogated FGF2-mediated rescue from these drug combinations. FGF2 also significantly mitigated cell cycle arrest and apoptosis induced by fulv/pictilisib

Figure 1. **Secreted protein screening reveals modulators of response to anti-estrogens, PI3Ki, and mTORC1i in ER+ breast cancer. (A)** Flowchart of screening approach. **(B)** In the discovery screen, MCF-7/GFP and T47D/GFP cells were treated with or without 1 µM fulv and each of 297 recombinant secreted proteins (at the documented ED_{50}) for 7 d. Medium, protein, and drug were refreshed on day 4. GFP fluorescence was measured on days 1 and 7. Background- and baseline-subtracted fluorescence values (day 7 fluorescence − day 1 fluorescence) were used to calculate a rescue z-score for each protein: (sample well fluorescence − mean fluorescence across plate)/SD. Red, pink, light blue, and dark blue points represent proteins that rescued from fulv ($z \geq 1$), partially rescued from fulv ($0.3 \leq z < 1$), partially sensitized to fulv ($-0.3 \geq z > -1$), or sensitized to fulv ($z \leq 1$), respectively. **(C)** In the validation screen, MCF-7 and T47D cells were treated with or without 1 µM fulv and dose ranges of 24 cytokines for 5 d. Relative viable cell numbers were measured using an SRB assay. Each square represents mean of duplicates. Rescue (%) is calculated as (cytokine-treated sample/no-cytokine sample) − 1. Cytokine names are colored by ability to rescue in B. **(D)** In the expansion screen, MCF-7, T47D, ZR75-1, and HCC-1500 cells were treated with or without 1 µM 4-hydroxytamoxifen (*T*), 1 µM fulv (*F*), 1 µM pictilisib (*P*), 20 nM everolimus (*E*), and dose ranges of 13 validated cytokines (from C) for 5 d. Cytokine names are colored by ability to rescue in B. Data were analyzed as in C. **(E)** Nine rescue hits from the discovery screen with complete mRNA and protein expression data were used to derive a TME Expression Score, which is the mean of z-scores calculated based on relative mRNA and protein (IHC) expression levels in ER+ breast TME tissues and cell types.

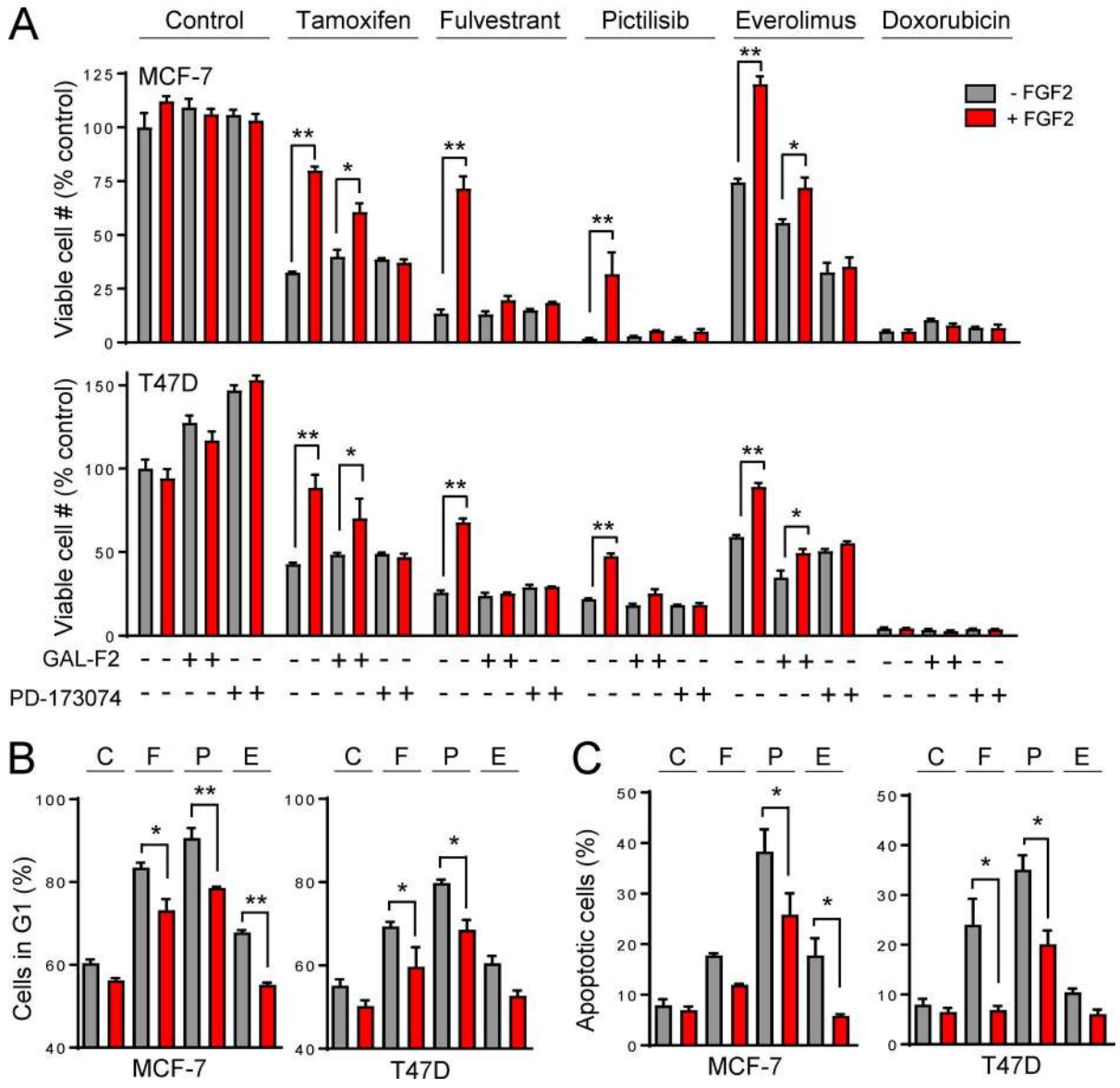

Figure 2. **FGF2 rescues ER+ breast cancer cells from anti-estrogens, PI3Ki, and mTORC1i in an FGFR-dependent manner. (A)** MCF-7 and T47D cells were pretreated for 1 h with or without 2 µg/ml GAL-F2 or 1 µM PD-173074 and then co-treated with or without 25 ng/ml FGF2 with or without 1 µM 4-hydroxytamoxifen, 1 µM fulv, 0.5 µM pictilisib, 40 nM everolimus, or 100 nM doxorubicin for 3 wk, with medium/drug refreshment twice weekly. Relative viable cell numbers were measured by crystal violet staining and quantification. **(B)** Cells were treated with or without 25 ng/ml FGF2, 1 µM fulv (F), 1 µM pictilisib (P), 20 nM everolimus (E), or control (C) for 3 d. Cells were analyzed for cell cycle profile by PI staining followed by flow cytometry. **(C)** Cells were treated as in B for 5 d and then analyzed for apoptosis by Annexin V/PI staining followed by flow cytometry. *, $P \leq 0.05$; **, $P < 0.0001$ by Bonferroni multiple comparison-adjusted post-hoc test. Red and gray bars indicate treatment with or without FGF2, respectively. Data are shown as a mean of triplicates + standard error.

or fulv/everolimus (Fig. 4, B and C). Drug target engagement and FGF2-induced FGFR-dependent phosphorylation of MEK1/2 and ERK1/2, Cyclin D1 up-regulation, and Bim down-regulation were validated by immunoblot analysis of FR cells (Figs. 4 D and S3 I). Bim knockdown suppressed apoptosis induced by fulv/pictilisib or fulv/everolimus and abrogated FGF2-mediated rescue (Fig. 4 E and Fig. S3, J and K). Knockdown of Cyclin D1 promoted G1 arrest and abrogated FGF2-mediated decreases in cell cycle arrest (Fig. 4 F and Fig. S3, L and M).

Therapeutic targeting of FGF2 inhibits growth of ER+ breast tumors

Recombinant human FGF2 injected subcutaneously is distributed systemically in mice (Katsouri et al., 2015). To determine whether FGF2 confers anti-estrogen resistance

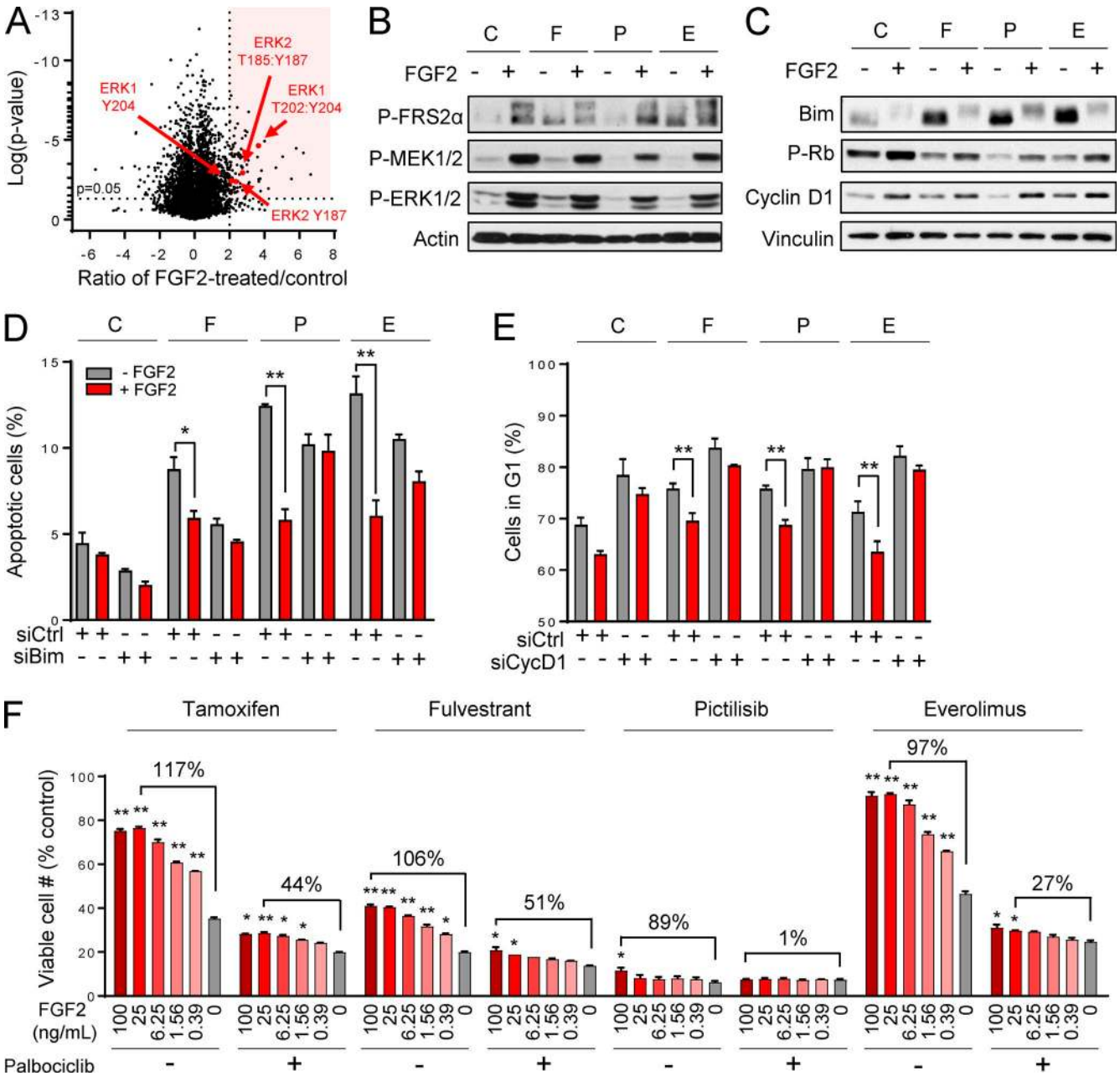

Figure 3. **FGF2 signaling activates MEK–ERK to suppress apoptosis through Bim down-regulation and promote proliferation through Cyclin D1 up-regulation. (A)** Phosphoproteomics was performed using SILAC coupled to LC-MS/MS in three pairs of samples: MCF-7 cells treated with or without 25 ng/ml FGF2 for 1 h, and MCF-7 and T47D cells pretreated with 1 µM fulv for 24 h and then treated with or without FGF2 for 1 h. Volcano plot of all phosphorylation events is shown. Pink shaded area represents phosphorylation events enriched more than twofold on average with $P \leq 0.05$ by Student's *t* test. Red dots represent all ERK1/2 phosphorylation sites. **(B and C)** MCF-7 cells were treated with or without 25 ng/ml FGF2, 1 µM fulv (F), 1 µM pictilisib (P), 40 nM everolimus (E), or control (C) for 24 h. Lysates were analyzed by immunoblot using the indicated antibodies. **(D and E)** MCF-7 cells were transfected with siRNA targeting nonsilencing control, Bim, or Cyclin D1. After 48 h, cells were treated with or without 25 ng/ml FGF2, 1 µM fulv (F), 0.5 µM pictilisib (P), or 40 nM everolimus (E) for 3 d. Cells were analyzed by flow cytometry as in Fig. 2 (B and C). **(F)** MCF-7 cells were pretreated with or without 1 µM palbociclib and then co-treated with 0–100 ng/ml FGF2 with or without 1 µM 4-hydroxytamoxifen, 1 µM fulv, 1 µM pictilisib, or 20 nM everolimus for 5 d. Relative viable cell numbers were measured using an SRB assay. Greatest fold changes between FGF2- and control-treated cells are indicated with brackets. Data in D–F are shown as mean of triplicates + SEM. *, $P \leq 0.05$; **, $P < 0.0001$ by Bonferroni multiple comparison-adjusted post-hoc test. Red/pink and gray bars indicate treatment with or without FGF2, respectively.

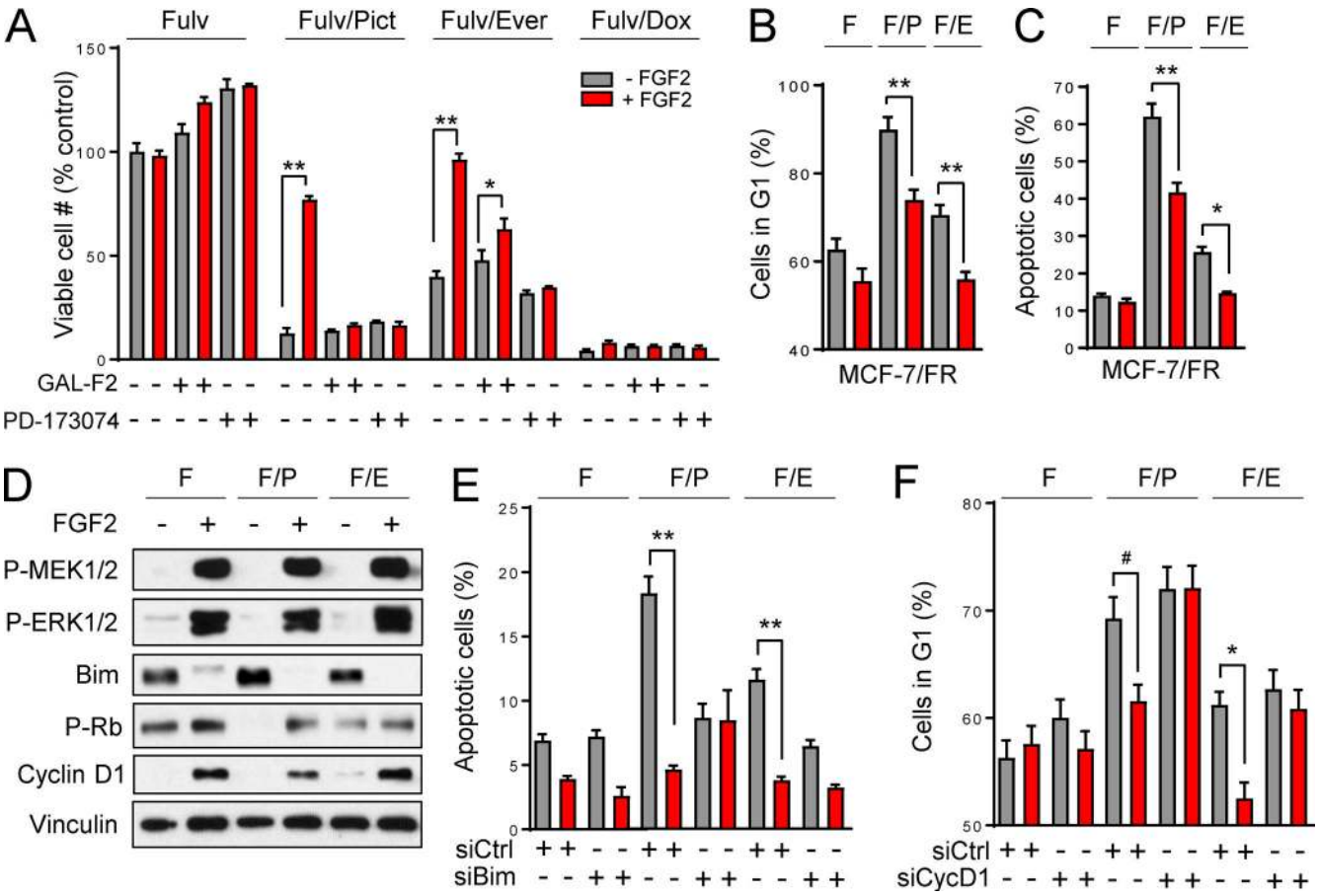

Figure 4. **FGF2 mediates resistance to PI3K/anti-estrogen and mTORC1/anti-estrogen combination therapies in anti-estrogen–resistant cells.** **(A)** Fulv-resistant MCF-7 cells (MCF7/FR) were pretreated for 1 h with or without GAL-F2 or PD-173074 and then co-treated with fulv (F) with or without 25 ng/ml FGF2, 1 µM pictilisib (P), 40 nM everolimus (E), or 100 nM doxorubicin (D) for 3 wk, with medium/drug refreshment twice weekly. Relative viable cell numbers were measured by crystal violet staining and quantification. **(B)** MCF7/FR cells were treated with fulv (F) with or without 25 ng/ml FGF2, 1 µM pictilisib (P), or 20 nM everolimus (E) for 3 d. Cells were analyzed for cell cycle profile by PI staining followed by flow cytometry. **(C)** MCF7/FR cells were treated with fulv (F) with or without 25 ng/ml FGF2, 1 µM pictilisib (P), or 20 nM everolimus (E) for 5 d. Cells were analyzed for apoptosis by Annexin V/PI staining followed by flow cytometry. **(D)** Cells were treated with fulv (F) with or without 25 ng/ml FGF2, 1 µM pictilisib (*P*), or 40 nM everolimus (*E*) for 24 h. Lysates were analyzed by immunoblot using the indicated antibodies. **(E and F)** MCF-7/FR cells were transfected with siRNA targeting nonsilencing control, Bim, or Cyclin D1. After 48 h, cells were treated with or without 25 ng/ml FGF2, 1 µM fulv (*F*), 0.5 µM pictilisib (*P*), or 40 nM everolimus (*E*) for 3 d. Cells were analyzed by flow cytometry as in B and C. All data are shown as mean of triplicates + SEM. *, $P \leq 0.05$; **, $P < 0.0001$; #, $P = 0.06$ by Bonferroni multiple comparison-adjusted post-hoc test. Red and gray bars indicate treatment with or without FGF2, respectively.

in vivo, immunodeficient mice bearing MCF-7 xenografts were randomized to treatment with vehicle, FGF2, fulv, or the combination. Although single-agent FGF2 did not affect growth of MCF-7 tumors, FGF2 significantly antagonized ($P = 3 \times 10^{-5}$) the growth-inhibitory effect of fulv (Figs. 5 A and S4 A). FGF2 significantly attenuated the antitumor effects of fulv on cell proliferation and apoptosis (detected by immunohistochemistry [IHC] for Ki67 and terminal deoxynucleotidyl transferase dUTP nick end labeling [TUNEL], respectively; Fig. 5, B and C; and Fig. S4 B). Immunoblot analysis of tumor lysates showed that fulv down-regulated ER levels and activity (assessed by decreased PR and Cyclin D1; Kastner et al., 1990; Altucci et al., 1996), whereas FGF2 activated FGFR–MEK–ERK signaling, rescued Cyclin D1 expression, and increased Rb phosphorylation (Fig. 5 D).

A more clinically relevant model requires modulation of endogenous FGF2 signaling in ER+ breast tumors. We therefore tested the effects of the FGF2-neutralizing antibody GAL-F2 in two models of ER+ breast cancer predicted to engage FGF2 signaling. 59-2-HI mouse ER+ mammary adenocarcinomas recruit stromal fibroblasts secreting high levels of endogenous FGF2 (Giulianelli et al., 2008). GAL-F2 was first confirmed to effectively block the drug-rescuing effects of mouse FGF2 in MCF-7 cells (Fig. S4 C). Immunocompetent, syngeneic mice bearing 59-2-HI tumors were randomized to treatment with vehicle, GAL-F2, fulv, or the combination. GAL-F2 synergized with fulv to suppress tumor growth (P

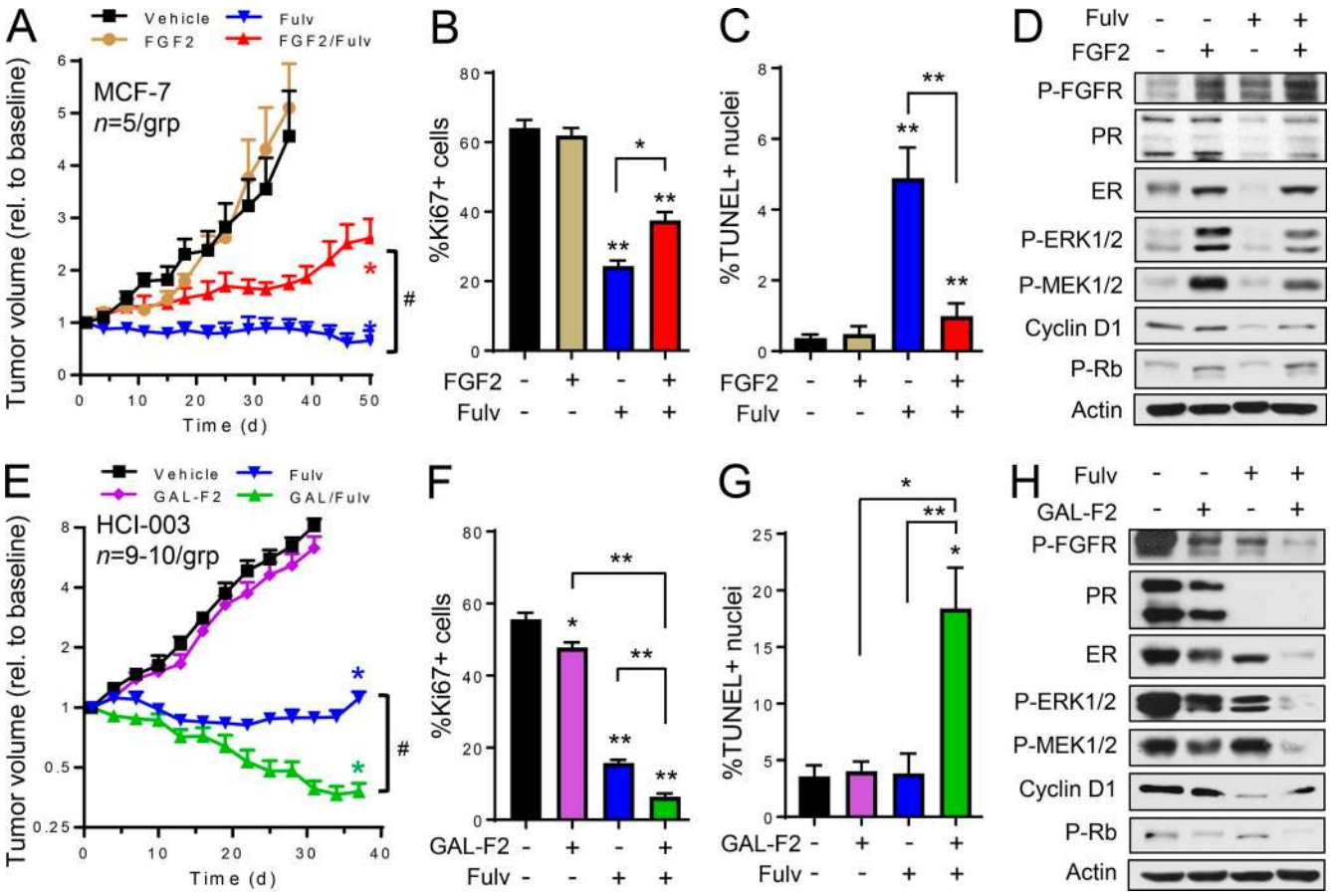

Figure 5. **FGF2 signaling mediates anti–estrogen resistance in mouse models of ER+ breast cancer.** Mice bearing MCF-7 xenografts **(A–D)** or HCI-003 xenografts **(E–H)** were randomized to the indicated treatments. In A and E, tumor growth data are shown as mean + SE. *, $P < 10^{-7}$ by linear mixed modeling compared with vehicle-treated group. In A, #antagonism $P = 3 \times 10^{-5}$. In E, #synergy $P = 1.7 \times 10^{-6}$. In B, C, F, and G, tumors harvested after 5 d of treatment were analyzed by IHC for Ki67 or TUNEL. Data are shown as mean + SEM. *, $P \leq 0.05$; **, $P < 0.0001$ by Bonferroni multiple comparison-adjusted post-hoc test compared with control unless otherwise indicated with brackets. In D and H, tumor lysates were analyzed by immunoblot using the indicated antibodies.

= 0.06), and the combination significantly inhibited growth compared with vehicle and single agents (all $P \leq 0.01$; Fig. S4, D and E). Ki67 IHC and TUNEL confirmed a significant decrease in proliferation and increase in apoptosis in fulv/GAL-F2 combination–treated tumors compared with those treated with vehicle or single agents (Fig. S4, F and G). Immunoblotting of tumor lysates confirmed that fulv and GAL-F2 decreased activation of ER and FGFR, respectively (Fig. S4 H).

HCI-003 was selected as an ER+ breast cancer patient-derived xenograft (PDX) with highest levels of FGFR–FRS2α–MEK–ERK pathway activation among six ER+ PDX models (Fig. S4 I). Mice bearing HCI-003 tumors were treated as in the 59-2-HI model. Fulv induced tumor stasis, whereas GAL-F2 synergized with fulv to induce tumor regression ($P = 1.7 \times 10^{-6}$; Figs. 5 E and S4 J). The combination of fulv/GAL-F2 more effectively inhibited tumor cell proliferation than either single agent, but the drug combination was required to induce apoptosis above baseline levels (Fig. 5, F and G; and Fig. S4 K). The drug combination also effectively blocked MEK–ERK activation and Rb phosphorylation in tumors, whereas single agents elicited partial effects (Fig. 5 H).

Because FGF2 can promote angiogenesis (Seghezzi et al., 1998), we assessed treatment effects on proportions of $CD31^+$ vascular endothelial cells in all three tumor models. FGF2 did not significantly alter endothelial cell numbers in MCF-7 tumors, and GAL-F2 treatment did not significantly alter endothelial cell numbers in 59-2-HI or HCI-003 tumors (Fig. S4 L). Thus, the anti-estrogen–rescuing effects of FGF2 in MCF-7 tumors and the antitumor effects of GAL-F2 in 59-2-HI and HCI-003 tumors are unlikely to be attributable to effects on angiogenesis.

Tumor transcriptomic profiles of FGF2 pathway activation predict early recurrence in patients with ER+ breast cancer

To determine whether FGF2 pathway activation is prognostic of survival and predictive of anti-estrogen resistance in humans, we performed RNA sequencing to generate tran-

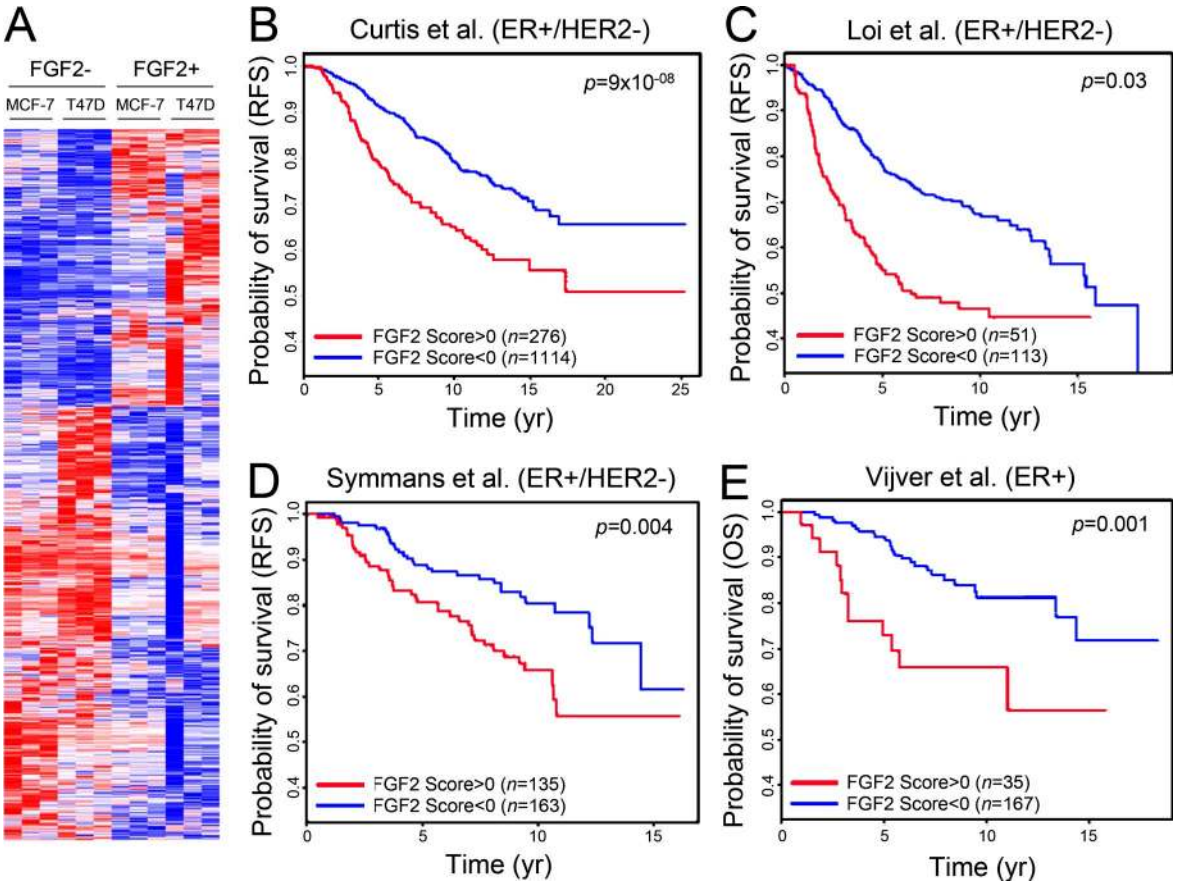

Figure 6. **FGF2 signaling is associated with poor disease outcome and anti–estrogen resistance in patients with ER+ breast cancer. (A)** MCF-7 and T47D cells were pretreated with 1 µM fulv for 24 h and then treated with or without 25 ng/ml FGF2 for 1 h in triplicate, and RNA sequencing was performed to generate a signature of FGF2 response. Heatmap of differentially expressed genes common between MCF-7 and T47D ($P < 0.05$) in response to FGF2 treatment. **(B–E)** RNA-sequencing data were used to derive FGF2 pathway activation scores for each human primary breast tumor from four independent datasets containing information from 1,390 (B), 164 (C), 298 (D), and 202 (E) patients. Patients with tumors exhibiting positive versus negative scores were compared by log-rank test using RFS (B–D) or OS (E).

scriptomic profiles of FGF2 response in MCF-7 and T47D cells treated ± FGF2 (Fig. 6 A). Gene set enrichment analyses (GSEAs) were performed using the hallmarks, oncogenic signatures, and motifs gene sets, and overlap of significant gene sets was determined between MCF-7 and T47D profiles. These analyses highlighted the importance of Rb/E2F signaling in FGF2 response and confirmed a putative role for MEK activation (Fig. S5, A–C).

A composite FGF2 signature was generated and used to calculate a FGF2 pathway activation score for each human primary ER+ breast tumor in four independent datasets containing information from 1,390, 164, 298, and 202 patients with ER+ breast cancer (van de Vijver et al., 2002; Loi et al., 2008; Symmans et al., 2010; Curtis et al., 2012); among these patients, 1,018/1,390 (73.2%), 164/164 (100%), 298/298 (100%), and 40/202 (19.8%) were treated with adjuvant anti-estrogen therapy. The first three datasets used recurrence-free survival (RFS) as an endpoint; the fourth dataset used overall survival (OS) as an endpoint. A positive score, indicative of relatively high FGF2 pathway activation, was significantly predictive of anti-estrogen resistance and shorter RFS in three datasets and prognostic of shorter OS in the fourth dataset (all $P \leq 0.03$; Fig. 6, B–E; and Fig. S5, D–G). Multivariate analysis of the largest dataset, which included clinical annotation, showed that FGF2 pathway activation score was predictive of RFS independently of age, tumor grade, stage, and *FGFR1/2/3/4* gene amplification status ($P = 0.008$; Table S3).

DISCUSSION

We screened a comprehensive microenvironmental secreted protein library to identify cytokines that modulate anti–estrogen sensitivity in ER+ breast cancer. We discovered and validated several cytokines that modulate sensitivity to fulv in vitro and further discovered that the same cytokines modulate sensitivity to 4-hydroxytamoxifen, PI3Ki, and mTORC1i across ER+ breast cancer cell lines. Using mRNA and protein expression data from normal tissues relevant to ER+

breast cancer, we developed a filter for our cytokine screen hits. Applying this filter highlighted FGF2 as the top validated cytokine that conferred resistance to both anti-estrogens and PI3K–mTOR pathway inhibitors and is highly expressed in ER+ breast cancer–relevant tissues and TME cell types. Indeed, several lines of evidence indicate that FGF2 is expressed in the ER+ breast TME: (a) FGF2 was observed in stroma in 34/54 (63%) breast tumors (Linder et al., 1998); (b) a broad range of FGF2 levels were detected in stroma, but not breast epithelial cells, in 149/149 (100%) breast tumors (Smith et al., 1999); and (c) FGF2 is robustly expressed by bone marrow stromal cells (Tivari et al., 2015), and bone is the most common site of metastasis for ER+ breast cancer. FGF2 IHC of tumors from four breast cancer patients confirmed FGF2 expression in stromal cells, including adipocytes, endothelial cells, and fibroblasts, but not cancer cells (Fig. S5 H). Here, we demonstrated that exogenous and endogenous FGF2 activates FGFR–MEK–ERK signaling to drive cell cycle progression and survival in ER+ breast cancer cells and tumors (modeled in Fig. 7), offering FGF2 as a potential TME-derived therapeutic target in ER+ breast cancer.

FGF2 modulates growth, differentiation, migration, and survival in a variety of normal and cancer cell types (Akl et al., 2016). In ER+ breast cancer, the role of FGF2 has been less clear. However, much progress has been made in characterizing and therapeutically targeting FGFR1 and FGFR2, which are genomically amplified in 10–15% and 1.6% of primary ER+ breast tumors, respectively (Cancer Genome Atlas Network, 2012). Amplification of *FGFR1* or *FGFR2* promotes ligand-independent kinase signaling in ER+ breast cancer cells (Reis-Filho et al., 2006), and *FGFR1* amplification is associated with anti-estrogen resistance (Turner et al., 2010). A phase II clinical trial testing the pan-FGFRi dovitinib as a single agent for metastatic ER+ breast cancer yielded unconfirmed partial responses in 3/20 patients with *FGFR1*-amplified tumors and provided similar rates of disease stabilization (45–48%) in both *FGFR1*-amplified and nonamplified cases (André et al., 2013). Furthermore, a subset analysis of a recent placebo-controlled randomized phase II trial (Musolino et al., 2017) revealed that combined fulv/dovitinib is more efficacious than fulv/placebo in patients with FGFR pathway–nonamplified (i.e., not amplified for *FGFR1*, *FGFR2*, or *FGF3*) advanced ER+ breast tumors; overall response rates were 31.3% (10/32) versus 8.8% (3/34; chi-square P = 0.03). Although limited by small sample size, these clinical data suggest that targeting FGFR in combination with anti-estrogens is a viable therapeutic strategy in FGFR pathway–nonamplified ER+ breast cancer. It should also be considered that ATP-competitive FGFRi frequently target multiple kinases (e.g., vascular endothelial growth factor receptor [VEGFR], platelet-derived growth factor receptor [PDGFR], and c-KIT), which may contribute to antitumor effects. Notably, three of the four parental ER+ breast cancer cell lines analyzed herein are *FGFR1* nonamplified.

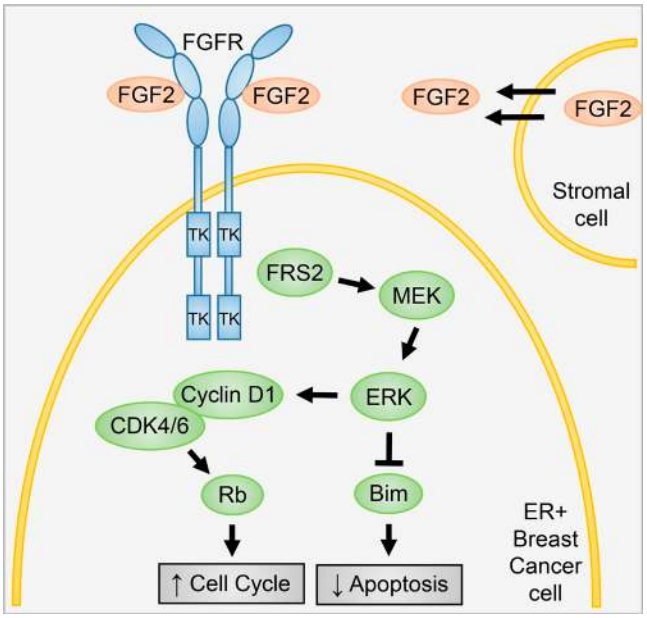

Figure 7. **Model of microenvironmental FGF2-mediated resistance in ER+ breast cancer.**

FGF2-mediated resistance to anti-estrogens, PI3Ki, and mTORC1i is a robust phenotype that applied to single-agent and combination therapies in anti-estrogen–sensitive and –resistant ER+ breast cancer cells but did not apply to doxorubicin. These results echo our prior work demonstrating that stromal cells more frequently confer cancer cell resistance to targeted therapeutics (e.g., kinase inhibitors) than conventional DNA-damaging agents (Straussman et al., 2012). Although PI3K–mTOR pathway inhibitors are approved or being developed to prevent/overcome anti–estrogen resistance, our screening data suggest that secretome-mediated drug resistance mechanisms are shared across anti-estrogens, PI3Ki, and mTORC1i. For example, FGF2 and NRG1 both strongly activate receptor tyrosine kinase and MAPK signaling (Wilson et al., 2012), suggesting that these ligands may elicit common downstream mechanisms of resistance to anti-estrogens, PI3Ki, and mTORC1i. In agreement with this concept, Kodack et al. (2017) recently reported that NRG1, which is expressed by both stromal and cancer cells within HER2+ and PIK3CA mutant breast cancer cell line–derived brain metastasis xenografts, confers resistance to PI3Ki. However, because of weak NRG1 expression in the normal tissues in our TME filter (Figs. S1, D and E), NRG1 was deprioritized in follow-up studies. The high degree of cross talk and antagonism between the ER and PI3K–mTOR pathways (Miller et al., 2011) further highlights the potential for common mechanisms of therapeutic resistance. However, other ligands known to activate ERK1/2, such as insulin-like growth factors and CXCL12 (SDF1α; Ma et al., 2015), were unable to rescue ER+ breast cancer cells from drug treatments (Fig. 1, C and D), im-

plying that resistance-conferring receptor–ligand signaling pathway subtleties require further mechanistic study.

FGF2 mitigated apoptosis induced by fulv, PI3Ki, and mTORC1i by decreasing levels of proapoptotic BH3-only protein Bim (Fig. 3, C and D; and Fig. S3, B–F), likely through ERK1/2-mediated phosphorylation (Hübner et al., 2008). Bim is thought to induce apoptosis by (a) sequestering antiapoptotic Bcl-2 family proteins (e.g., Bcl-2 and Bcl-xL) away from Bax and Bak, which form pores in the mitochondrial outer membrane to induce cytochrome *c* release, and/or (b) binding Bax/Bak directly in the mitochondrial outer membrane (Huang and Strasser, 2000). Vaillant et al. (2013) showed that BH3 mimetics such as ABT-737 induce Bim release from Bcl-2/Bcl-xL and synergize with tamoxifen and a dual PI3Ki/mTORi in models of ER+ breast cancer, offering BH3 mimetics as a potential approach to abrogate FGF2-mediated drug resistance.

FGF2 induced up-regulation of Cyclins, phosphorylation of Rb, activation of Rb/E2F transcriptional programs, and mitigation of G1 arrest to confer resistance to anti-estrogens, PI3Ki, and mTORC1i in a Cyclin D1–dependent manner (Fig. 3, C and E; and Fig. 5 B; and Fig. S3, A, B, and H). Cyclin D1 and CDK4 are required for mammary tumor growth in mice (Yu et al., 2001, 2006). Cyclin D1 is encoded by an estrogen-inducible ER target gene (*CCND1*) that promotes cell cycle progression in ER+ breast cancer cells (Foster et al., 2001). Furthermore, *CCND1* is commonly amplified or overexpressed in ER+ breast cancers (Cancer Genome Atlas Network, 2012), and increased activation of the Cyclin D1–CDK4/6–Rb axis drives anti-estrogen resistance (Wilcken et al., 1997; Bosco et al., 2007; Rudas et al., 2008). CDK4/6 inhibition with palbociclib, which is approved for the treatment of advanced ER+ breast cancer in combination with anti-estrogens (Turner et al., 2015; Finn et al., 2016), abrogated FGF2-mediated rescue from anti-estrogens, PI3Ki, and mTORC1i (Figs. 3 F and S3 H). These data suggest that FGF2-mediated rescue requires CDK4/6 signaling and that the clinical success of CDK4/6i may be mediated in part by circumvention of FGF2-mediated drug resistance. Similarly, our findings suggest that combining palbociclib with anti-estrogen/everolimus doublet therapy represents a rational strategy to abrogate resistance to the doublet that is being tested in ongoing clinical trials (e.g., NCT02871791).

Interestingly, phosphorylation of transcription factor FOXO3a at S284, a putative inhibitory ERK1/2 phosphorylation site (Dephoure et al., 2008), was the phosphorylation site with the largest fold change in the FGF2-treated samples (Table S2). FOXO3a has previously been implicated in both induction of Bim expression and inhibition of Cyclin D1 transcription (Huang and Tindall, 2007) and thus is a potential transcription factor candidate immediately downstream of ERK1/2 responsible for FGF2-mediated resistance. The specific mechanism by which ERK1/2 leads to degradation of Bim and up-regulation of Cyclin D1, whether through FOXO3a or another transcriptional program, will be the subject of future study.

In summary, microenvironmental secreted factor screening revealed cytokines that modulate drug sensitivity in ER+ breast cancer cells. FGF2 is prominently expressed in ER+ breast cancer–relevant tissues and cell types and confers resistance to anti-estrogens, PI3Ki, and mTORC1i. The clinical relevance of this phenotype was confirmed in analyses of four patient cohorts and three ER+ breast tumor models, highlighting FGF2/FGFR signaling as a potential therapeutic opportunity in FGFR pathway–nonamplified ER+ breast cancer.

MATERIALS AND METHODS

Cell lines and RNA interference

Parental cell lines were obtained from ATCC and cultured in DMEM/10% FBS (Hyclone). FR cells were maintained in 1 μM fulv (Tocris Bioscience). MCF-7/FR cells were a gift from M. Ellis (Baylor College of Medicine, Houston, TX). ZR75-1/FR cells were generated by culturing ZR75-1 cells with 1 μM fulv for 4 mo. Cells were transfected with siRNA targeting Bim (Dharmacon, Qiagen), Cyclin D1 (Ambion), or nonsilencing control (Qiagen) using Lipofectamine RNAiMAX (Life Technologies) per the manufacturer's instructions.

Cytokine screening

Commercially available human proteins (n = 297) predicted to be secreted (Chen et al., 2005) were used in the discovery screen; the full contents of this screen are being reported in a separate publication. GFP-labeled MCF-7 and T47D cells (1,700 cells/well in 40 μl) were plated in 384-well plates. The next day, cells were treated with 10 μl of the 6× cytokine library and 10 μl of 6× (6 μM) fulv. 3 d later, medium, cytokines, and drug were refreshed. GFP fluorescence was measured on days 1 and 7. Background- and baseline-subtracted fluorescence values (day 7 GFP fluorescence − day 1 GFP fluorescence) were used to calculate discovery rescue z-scores: z = (sample well fluorescence − mean fluorescence across plate)/SD.

For the validation and expansion screens, 24 recombinant cytokines were purchased from Peprotech (Table S2). Short-term (5-d) relative cell growth was quantified by SRB assay and used to quantify validation rescue score, calculated as (cytokine-treated sample/no cytokine sample) − 1.

Long-term growth assays

Cells were seeded in triplicate in 12-well plates (3,000 cells/well). The next day, cytokine and/or drug was added as indicated. Medium, cytokines, and drugs were refreshed every 3–4 d. When a well either reached ∼90% confluence, or after 8 wk, adherent cells were fixed and stained with 0.5% crystal violet in 20% methanol. Scanned images were quantified using the ColonyArea plugin in ImageJ (Guzmán et al., 2014).

Microenvironment bioinformatics filter

RNA-sequencing data were downloaded from the Genotype Tissue Expression (GTEx) project (GTEx Consortium, 2015), and protein IHC-based expression data were obtained from The Human Protein Atlas (THPA) project (Uhlén et al., 2015).

Data were reported as mRNA level (log_{10}[RPKM]; normalized to whole blood) and protein level (3 = high, 2 = medium, 1 = low, 0 = none; normalized to median expression in all tissues). Protein expression score is based on immunohistochemical data manually scored for staining intensity (negative, weak, moderate, or strong) and fraction of stained cells (<25%, 25–75%, or >75%). Staining intensity and fraction of staining is then converted into a protein expression level score (absent, negative or weak <25%; low, weak 25–75%, weak >75%, or moderate <25%; medium, moderate 25–75%, moderate >75%, or strong <25%; high, strong 25–75%, or strong >75%). We focused on mRNA and protein expression levels in breast tissue components (breast mammary, adipose, and primary fibroblasts) and common metastatic sites of ER+ breast cancer (bone marrow, lung, and liver), with equal weight assigned to each of these tissue sites. For the 14 cytokines with a rescue z-score ≥1 in the discovery screen, mRNA and protein expression z-scores were calculated as follows: z_{mRNA} = (gene expression of secreted factor − mean gene expression of 14 secreted factors)/SD and z_{prot} = (protein expression of secreted factor − mean protein expression of nine secreted factors)/SD. Protein expression data were unavailable for 5/14 cytokines. Gene and protein expression z-scores were averaged to calculate a composite TME z-score for the remaining nine cytokines (Fig. 1 E).

Apoptosis assay

Cells seeded in triplicate in 6-well plates (5×10^4 cells/well) were treated as indicated for 5 d. Floating and adherent cells (dislodged by trypsinization) were processed using the ApoScreen Annexin Apoptosis kit (Southern Biotech) and analyzed by flow cytometry with FlowJo software. Cells staining positively for Annexin V were considered apoptotic. For siRNA experiments, at 2 d after transfection, cells were treated with ligands/drugs as indicated for 3 d.

Cell cycle profiling

Cells seeded in triplicate in 6-well plates (7.5×10^4 cells/well) were treated as indicated for 3 d. Floating and adherent cells (dislodged by trypsinization) were fixed in 70% ethanol overnight, stained with propidium iodide (PI; Southern Biotech), and analyzed by flow cytometry. Proportions of cells in G1, S, or G2/M phase were modeled using Modfit LT (Verity Software House).

Immunoblotting

Cells were lysed, and frozen tumors were homogenized and lysed in RIPA buffer (20 mM Tris, pH 7.4, 150 mM NaCl, 1% NP-40, 10% glycerol, 1 mM EDTA, 1 mM EGTA, 5 mM NaPPi, 50 mM NaF, 10 mM Na β-glycerophosphate, plus fresh Halt protease inhibitor cocktail; Pierce; and 1 mM Na_3VO_4; New England Biolabs). Lysates were sonicated for 15 s and centrifuged at 17,000 *g* for 10 min at 4°C, and protein in supernatants was quantified using BCA assay (Pierce). Lysates were denatured with NuPage (Life Technologies) and reduced with 1.25% β-mercaptoethanol (Sigma). Proteins were separated by SDS-PAGE and transferred to nitrocellulose. Even protein loading across lanes was visually confirmed with Ponceau S staining. Blots were probed with antibodies against P-AKT_{S473}, P-AKT_{T308}, P-$p70S6K_{T389}$, P-$S6_{S240/244}$, P-$ERK1/2_{T202/Y204}$, P-$MEK1/2_{S217/221}$, Cyclin D1, Bim, Bcl-2, Bcl-xL, Mcl-1, PUMA, P-$Stat3_{Y705}$, actin, vinculin (Cell Signaling), ER, Cyclin A, Cyclin B1, Bad, Bax (Santa Cruz), Bak (Upstate), and PR (Dako). Antibodies against Cyclin A, Cyclin B1, Bad, Bax, and Bak were provided by A. Eastman (Geisel School of Medicine, Lebanon, NH). HRP-labeled secondary antibodies (GE Healthcare) and ECL or ELISA Pico substrate (Thermo Scientific) were used for signal detection.

IHC

5-µm sections of FFPE tissue were used for H&E staining, IHC with Ki67 antibody (Biocare Medical), TUNEL (DeadEnd Colorimetric System; Promega), or CD31 (BD Biosciences). Proportions of positively stained cells were counted in three random microscopic fields (400× magnification) in each specimen using ImageJ. Quantification of IHC for Ki67 and TUNEL was performed using the NIH ImageJ plugin IHC Image Analysis Toolbox. Quantification of IHC for CD31 was performed using NIH ImageJ as previously described (Owens et al., 2010). IHC images for human breast tumors were obtained from THPA (Uhlén et al., 2015), and images from four representative breast tumors (two ductal and two lobular adenocarcinomas) were examined and analyzed by a collaborating board-certified pathologist with expertise in breast cancer (J. Marotti).

SILAC and phosphoproteomics

Cells were grown in heavy or light DMEM (Gibco) supplemented with 10% dialyzed FBS (Hyclone) for six doublings as described previously (Petrone et al., 2016). Heavy medium contained 100 mg/L $^{13}C_6{}^{15}N_2$-lysine and 100 mg/L $^{13}C_6{}^{15}N_4$-arginine (Cambridge Isotope Laboratories). Light medium contained 100 mg/L $^{12}C_6{}^{14}N_2$-lysine and 100 mg/L $^{12}C_6{}^{14}N_4$-arginine (Sigma). Cells were treated as indicated +/− 1 µM fulv for 24 h. Heavy- and light-labeled cells were treated with or without 25 ng/ml FGF2 for 1 h, respectively. Cells were lysed, protein was quantified, and paired protein lysates were mixed at a 1:1 ratio. After trypsin digestion, phosphopeptides were enriched from mixtures using TiO_2 microspheres and analyzed by liquid chromatography tandem mass spectrometry (LC-MS/MS) as described previously (Petrone et al., 2016). Log2 heavy/light ratios were median adjusted for mixing errors. Phosphopeptide fold changes were adjusted for changes in protein abundance on a per-sample basis. Significance of log_2 protein-corrected phosphopeptide fold change among the three experiments was determined by two-tailed Student's *t* test assuming unequal variance. Motif analysis of residues with increased phosphorylation (more than twofold, $P < 0.05$) in the presence of FGF2 was performed using MMFPh (maximal motif finder for phosphoproteomics datasets; Wang et al., 2012b).

RNA sequencing

MCF-7 and T47D cells were pretreated with or without 1 μM fulv for 24 h and then co-treated with or without 25 ng/ml FGF2 for 1 h in triplicate. RNA extraction and DNase digestion were performed using RNeasy Mini Kit (Qiagen). RNA quality was assessed on a fragment analyzer (Advanced Analytical Technologies), and RNA was quantified by Qubit. Ribo-depleted RNA-sequencing libraries were prepared from 2.5 μg of total RNA using the GlobinZero gold (GZG1206; Illumina) and TruSeq Stranded Total RNA (RS-122-2201; Illumina) workflows according to the manufacturer's instructions. Each library was uniquely barcoded, quantified by quantitative PCR (KK4824; Kapa Biosystems) and pooled for sequencing on an Illumina NextSeq500 (2 × 75-bp run). RNA sequencing data were analyzed using the TruSeq Stranded RNA-Seq pipeline by Partek as follows: (a) RNA sequencing data were trimmed from the 3′ end with a Phred score cutoff of 20; (b) sequences were aligned to the hg19 reference human genome using STAR aligner (STAR 2.4.1d; Dobin et al., 2013); (c) transcripts were filtered to exclude transcripts with maximum raw read counts ≤20, and transcript-level expression was quantified using Partek E/M (Xing et al., 2006); and (d) transcript read counts were normalized using the trimmed mean of M values +1 algorithm (Robinson and Oshlack, 2010). A heatmap was generated using Morpheus (Broad Institute). Data are available at the NCBI BioProject website under accession number 389319.

FGF2 pathway activation scoring and patient survival analyses

Human ER+ breast tumor gene expression datasets were downloaded from the European Genome-Phenome archive (METABRIC; EGAS00000000083; Curtis et al., 2012), the Gene Expression Omnibus (accession nos. GSE9195, GSE6532, and GSE17705; Loi et al., 2008; Symmans et al., 2010), and the Netherlands Cancer Institute (http://ccb.nki.nl/data/; van de Vijver et al., 2002). To determine the weights used in the FGF2 Pathway Activation profile, the $\log_2$ fold-change in gene expression was calculated by comparing MCF-7 and T47D cells treated with fulv with or without FGF2. A composite $\log_2$ fold-change profile was created by taking the mean $\log_2$ fold change of each gene across both cell types; this yielded three profiles of MCF-7 only, T47D only, or MCF-7/T47D averaged. These fold-change profiles were then z-transformed to follow a normal distribution. Each z-score profile was then split into an up-regulated and down-regulated profile depending on whether the z-score was above or below zero. The z-scores in each up-regulated and down-regulated vector were then converted to a p-value and $-\log_{10}$ transformed. To minimize the effect of extreme values, all log-transformed p-values >10 were trimmed to 10. All values were then rescaled to between 0 and 1 by dividing by the maximum value in the dataset.

FGF2 pathway activation scores for each tumor were calculated by inputting the gene expression profile's respective weight vectors into the binding association with sorted expression (BASE) algorithm (Cheng et al., 2007). The full details of this profile calculation have been described previously (Varn et al., 2015). For survival analyses, patients were stratified into high versus low FGF2 pathway activation groups based on whether their scores were above or below zero. The survival distributions of the two groups were then compared using a log-rank test and visualized using a Kaplan-Meier plot. To adjust for additional clinical factors available in the METABRIC dataset, each group was regressed using a multivariate Cox proportional hazards model with age, stage, grade, and *FGFR1/2/3/4* amplification status as covariates. All survival analyses were performed in the R programming language using the "survival" package.

GSEA

GSEA was performed using GSEA 3.0 on the javaGSEA Desktop Application (Subramanian et al., 2005). chip and cls files were generated according to the GSEA User Guide. FGF2-positive samples were compared with FGF2-negative samples separately for MCF-7 and T47D using the hallmarks (H), motifs (C3), and oncogenic signatures gene sets (C6). 1,000 permutations were performed for each analysis using the default settings.

Mouse studies

Female NOD-scid/IL2R$\gamma^{-/-}$ (NSG) mice were obtained from the Norris Cotton Cancer Center Transgenic and Genetic Construct Shared Resource. Female athymic (J:Nu) and BALB/cJ mice were obtained from The Jackson Laboratory. MCF-7 cells (~5×10^6) were injected s.c. into athymic mice. Fragments (~8 mm^3) of 59-2-HI mouse adenocarcinoma tumor tissue (Giulianelli et al., 2008; gift from C. Lanari, National Scientific and Technical Research Council, Buenos Aires, Argentina) were inserted s.c. into ovariectomized BALB/cJ mice. Fragments of HCI-003 PDX tissue (DeRose et al., 2011; gift from A. Welm, University of Utah, Salt Lake City, UT) were orthotopically implanted into the inguinal mammary fat pad of NSG mice. Mice implanted with MCF-7 cells or HCI-003 fragments were also implanted s.c. with a 1-mg beeswax 17β-estradiol pellet (DeRose et al., 2013). Tumor volumes were measured twice weekly using calipers (volume = length × $width^2/2$). Mice bearing MCF-7 tumors ~200 mm^3 were randomized to treatment with vehicle (100 μl/d s.c.; PBS [for FGF2] or castor oil [for fulv]), human FGF2 (20 μg/kg/d s.c.; Katsouri et al., 2015; Peprotech), fulv (5 mg/wk s.c.; AstraZeneca), or the combination. Mice bearing 59-2-HI or HCI-003 tumors ~150 mm^3 were randomized to treatment with vehicle (100 μl/d s.c.; castor oil [for fulv] or mouse IgG [for GAL-F2]), fulv, GAL-F2 [5 mg/kg twice weekly i.p.; Galaxy Biotech; Wang et al., 2012a), or the combination. Tumors were harvested and cut in pieces for snap freezing or formalin fixation followed by paraffin embedding.

Statistics

For cell growth, apoptosis, cell cycle profiling, IHC, and TUNEL assays, data were analyzed by ANOVA with Bonferroni multiple comparison-adjusted post-hoc testing between groups. Triplicates shown for cell growth, apoptosis, and cell cycle profiling in figures were done as replicate samples within the same experiments, with findings repeated in at least two independent experiments for most figures to validate the data. To estimate progression/regression of tumors, the following linear mixed model was employed: $\log_{10}(\text{tumor volume}_{it}) = a_i + b*t + e_{it}$, where i represents the i^{th} mouse, t represents the time of tumor volume measurement, a_i represents the mouse-specific log tumor volume at baseline (t = 0), slope b represents rate of tumor volume growth (or reduction), and e_{it} represents deviation of measurements from the model over time (Demidenko, 2006, 2010, 2013). The variance of a_i is interpreted as mouse heterogeneity, and $b*\log_e(10) \times 100$ estimates the percent tumor volume increase per week. The computation was performed in R, using function "lme" from library "nlme." Treatment groups were compared using a z test for slopes with standard error derived from lme. Synergy and antagonism were assessed using the difference of slopes $(b_1 - b_0) + (b_2 - b_0) - (b_{12} - b_0)$, where b_1, b_2, b_{12}, and b_0 are the slopes from treatment groups 1, 2, the combined treatment, and the control group, respectively.

Study approval

Animal studies were approved by the Dartmouth College Institutional Animal Care and Use Committee.

Online supplemental material

Fig. S1 shows additional results from the tumor microenvironmental screening and bioinformatic filter approaches. Fig. S2 shows cell growth, proteomics, and immunoblot assays used to validate drug targets and confirm MAPK-pathway involvement in FGF2-mediated resistance. Fig. S3 shows immunoblot, flow cytometry, and cell growth assays to confirm FGF2-mediated suppression of apoptosis through Bim down-regulation and promotion of proliferation through Cyclin D1 up-regulation. Fig. S4 shows supplemental data for the MCF-7 and HCI-003 xenograft models and complete data for the 59-2-HI allograft model. Fig. S5 shows gene set enrichment and patient survival analyses of ±FGF2 RNA sequencing data and IHC expression of FGF2 in patient tumors. Tables S1, S2, and S3 are provided as Excel tables. Table S1 shows screen results of cytokines used in the validation screen. Table S2 shows phosphoprotein profiling results. Table S3 shows that the tumor transcriptomic profile of FGF2 pathway activation is associated with RFS independent of age, tumor grade, stage, and tumor *FGFR* gene amplification status.

ACKNOWLEDGMENTS

We thank Alana Welm for sharing the HCI-003 tumor model, Claudia Lanari for sharing the 59-2-HI tumor model, and Alan Eastman for sharing antibodies. We also thank Jonathan Marotti, a board-certified pathologist, for reviewing IHC slides. We thank the following Norris Cotton Cancer Center Shared Resources for assistance: mouse modeling, genomics and molecular biology, pathology, flow cytometry, microscopy, and biostatistics.

Funding support was provided by the American Cancer Society (RSG-13-292-01-TBE to T.W. Miller), the National Institutes of Health (F30CA216966 to K. Shee, R01CA211869 to T.W. Miller, and R35GM119455 to A.N. Kettenbach), and the Dartmouth College Norris Cotton Cancer Center (support grant P30CA023108).

The authors declare no competing financial interests.

Author contributions: K. Shee, T.R. Golub, R. Straussman, A.N. Kettenbach, and T.W. Miller designed the research. K. Shee, W. Yang, J.W. Hinds, R.A. Hampsch, K. Patel, N.A. Traphagen, F.S. Varn, C. Cheng, N.P. Jenkins, E. Demidenko, and P. Owens performed the experiments and analyzed data. A.C. Faber provided reagents. K. Shee and T.W. Miller wrote the manuscript. All authors read and approved the final manuscript.

Submitted: 3 October 2017

Revised: 29 December 2017

Accepted: 1 January 2018

REFERENCES

Akl, M.R., P. Nagpal, N.M. Ayoub, B. Tai, S.A. Prabhu, C.M. Capac, M. Gliksman, A. Goy, and K.S. Suh. 2016. Molecular and clinical significance of fibroblast growth factor 2 (FGF2 /bFGF) in malignancies of solid and hematological cancers for personalized therapies. *Oncotarget.* 7:44735–44762. https://doi.org/10.18632/oncotarget.8203

Altucci, L., R. Addeo, L. Cicatiello, S. Dauvois, M.G. Parker, M. Truss, M. Beato, V. Sica, F. Bresciani, and A. Weisz. 1996. 17beta-Estradiol induces cyclin D1 gene transcription, p36D1-p34cdk4 complex activation and p105Rb phosphorylation during mitogenic stimulation of G(1)-arrested human breast cancer cells. *Oncogene.* 12:2315–2324.

American Cancer Society. 2015. Cancer Facts & Figures 2015. American Cancer Society, Atlanta, GA. 56 pp.

André, F., T. Bachelot, M. Campone, F. Dalenc, J.M. Perez-Garcia, S.A. Hurvitz, N. Turner, H. Rugo, J.W. Smith, S. Deudon, et al. 2013. Targeting FGFR with dovitinib (TKI258): preclinical and clinical data in breast cancer. *Clin. Cancer Res.* 19:3693–3702. https://doi.org/10.1158/1078-0432.CCR-13-0190

Bosco, E.E., Y. Wang, H. Xu, J.T. Zilfou, K.E. Knudsen, B.J. Aronow, S.W. Lowe, and E.S. Knudsen. 2007. The retinoblastoma tumor suppressor modifies the therapeutic response of breast cancer. *J. Clin. Invest.* 117:218–228. https://doi.org/10.1172/JCI28803

Cancer Genome Atlas Network. 2012. Comprehensive molecular portraits of human breast tumours. *Nature.* 490:61–70. https://doi.org/10.1038/nature11412

Caunt, C.J., M.J. Sale, P.D. Smith, and S.J. Cook. 2015. MEK1 and MEK2 inhibitors and cancer therapy: the long and winding road. *Nat. Rev. Cancer.* 15:577–592. https://doi.org/10.1038/nrc4000

Chen, Y., Y. Zhang, Y. Yin, G. Gao, S. Li, Y. Jiang, X. Gu, and J. Luo. 2005. SPD--a web-based secreted protein database. *Nucleic Acids Res.* 33:D169–D173. https://doi.org/10.1093/nar/gki093

Cheng, C., X. Yan, F. Sun, and L.M. Li. 2007. Inferring activity changes of transcription factors by binding association with sorted expression profiles. *BMC Bioinformatics.* 8:452. https://doi.org/10.1186/1471-2105-8-452

Curtis, C., S.P. Shah, S.F. Chin, G. Turashvili, O.M. Rueda, M.J. Dunning, D. Speed, A.G. Lynch, S. Samarajiwa, Y. Yuan, et al. METABRIC Group. 2012. The genomic and transcriptomic architecture of 2,000 breast tumours reveals novel subgroups. *Nature.* 486:346–352.

Demidenko, E. 2006. The assessment of tumour response to treatment. *Appl. Stat.* 55:365–377.

Demidenko, E. 2010. Three endpoints of in vivo tumour radiobiology and their statistical estimation. *Int. J. Radiat. Biol.* 86:164–173. https://doi.org/10.3109/09553000903419304

Demidenko, E. 2013. Mixed Models: Theory and Applications with R. John Wiley & Sons, Hoboken, NJ. 717 pp.

Dephoure, N., C. Zhou, J. Villén, S.A. Beausoleil, C.E. Bakalarski, S.J. Elledge, and S.P. Gygi. 2008. A quantitative atlas of mitotic phosphorylation. *Proc. Natl. Acad. Sci. USA.* 105:10762–10767. https://doi.org/10.1073/pnas.0805139105

DeRose, Y.S., G. Wang, Y.C. Lin, P.S. Bernard, S.S. Buys, M.T. Ebbert, R. Factor, C. Matsen, B.A. Milash, E. Nelson, et al. 2011. Tumor grafts derived from women with breast cancer authentically reflect tumor pathology, growth, metastasis and disease outcomes. *Nat. Med.* 17:1514–1520. https://doi.org/10.1038/nm.2454

DeRose, Y.S., K.M. Gligorich, G. Wang, A. Georgelas, P. Bowman, S.J. Courdy, A.L. Welm, and B.E. Welm. 2013. Patient-derived models of human breast cancer: protocols for in vitro and in vivo applications in tumor biology and translational medicine. *Curr. Protoc. Pharmacol.* Chapter 14:Unit14.23.

Dobin, A., C.A. Davis, F. Schlesinger, J. Drenkow, C. Zaleski, S. Jha, P. Batut, M. Chaisson, and T.R. Gingeras. 2013. STAR: ultrafast universal RNA-seq aligner. *Bioinformatics.* 29:15–21. https://doi.org/10.1093/bioinformatics/bts635

Early Breast Cancer Trialists' Collaborative Group (EBCTCG), Davies, C., J. Godwin, R. Gray, M. Clarke, D. Cutter, S. Darby, P. McGale, H.C. Pan, C. Taylor, Y.C. Wang, et al. 2011. Relevance of breast cancer hormone receptors and other factors to the efficacy of adjuvant tamoxifen: patient-level meta-analysis of randomised trials. *Lancet.* 378:771–784. https://doi.org/10.1016/S0140-6736(11)60993-8

Ferlay, J., H.R. Shin, F. Bray, D. Forman, C. Mathers, and D.M. Parkin. 2010. Estimates of worldwide burden of cancer in 2008: GLOBOCAN 2008. *Int. J. Cancer.* 127:2893–2917. https://doi.org/10.1002/ijc.25516

Ferlay, J., I. Soerjomataram, R. Dikshit, S. Eser, C. Mathers, M. Rebelo, D.M. Parkin, D. Forman, and F. Bray. 2015. Cancer incidence and mortality worldwide: sources, methods and major patterns in GLOBOCAN 2012. *Int. J. Cancer.* 136:E359–E386. https://doi.org/10.1002/ijc.29210

Fidler, I.J., C. Wilmanns, A. Staroselsky, R. Radinsky, Z. Dong, and D. Fan. 1994. Modulation of tumor cell response to chemotherapy by the organ environment. *Cancer Metastasis Rev.* 13:209–222. https://doi.org/10.1007/BF00689637

Finn, R.S., M. Martin, H.S. Rugo, S. Jones, S.A. Im, K. Gelmon, N. Harbeck, O.N. Lipatov, J.M. Walshe, S. Moulder, et al. 2016. Palbociclib and Letrozole in Advanced Breast Cancer. *N. Engl. J. Med.* 375:1925–1936. https://doi.org/10.1056/NEJMoa1607303

Foster, J.S., D.C. Henley, A. Bukovsky, P. Seth, and J. Wimalasena. 2001. Multifaceted regulation of cell cycle progression by estrogen: regulation of Cdk inhibitors and Cdc25A independent of cyclin D1-Cdk4 function. *Mol. Cell. Biol.* 21:794–810. https://doi.org/10.1128/MCB.21.3.794-810.2001

Giulianelli, S., J.P. Cerliani, C.A. Lamb, V.T. Fabris, M.C. Bottino, M.A. Gorostiaga, V. Novaro, A. Góngora, A. Baldi, A. Molinolo, and C. Lanari. 2008. Carcinoma-associated fibroblasts activate progesterone receptors and induce hormone independent mammary tumor growth: A role for the FGF-2/FGFR-2 axis. *Int. J. Cancer.* 123:2518–2531. https://doi.org/10.1002/ijc.23802

GTEx Consortium. 2015. Human genomics. The Genotype-Tissue Expression (GTEx) pilot analysis: multitissue gene regulation in humans. *Science.* 348:648–660. https://doi.org/10.1126/science.1262110

Guzmán, C., M. Bagga, A. Kaur, J. Westermarck, and D. Abankwa. 2014. ColonyArea: an ImageJ plugin to automatically quantify colony formation in clonogenic assays. *PLoS One.* 9:e92444. https://doi.org/10.1371/journal.pone.0092444

Hay, M., D.W. Thomas, J.L. Craighead, C. Economides, and J. Rosenthal. 2014. Clinical development success rates for investigational drugs. *Nat. Biotechnol.* 32:40–51. https://doi.org/10.1038/nbt.2786

Huang, D.C., and A. Strasser. 2000. BH3-Only proteins-essential initiators of apoptotic cell death. *Cell.* 103:839–842. https://doi.org/10.1016/S0092-8674(00)00187-2

Huang, H., and D.J. Tindall. 2007. Dynamic FoxO transcription factors. *J. Cell Sci.* 120:2479–2487. https://doi.org/10.1242/jcs.001222

Hübner, A., T. Barrett, R.A. Flavell, and R.J. Davis. 2008. Multisite phosphorylation regulates Bim stability and apoptotic activity. *Mol. Cell.* 30:415–425. https://doi.org/10.1016/j.molcel.2008.03.025

Kastner, P., A. Krust, B. Turcotte, U. Stropp, L. Tora, H. Gronemeyer, and P. Chambon. 1990. Two distinct estrogen-regulated promoters generate transcripts encoding the two functionally different human progesterone receptor forms A and B. *EMBO J.* 9:1603–1614.

Katsouri, L., A. Ashraf, A.M. Birch, K.K. Lee, N. Mirzaei, and M. Sastre. 2015. Systemic administration of fibroblast growth factor-2 (FGF2) reduces BACE1 expression and amyloid pathology in APP23 mice. *Neurobiol. Aging.* 36:821–831. https://doi.org/10.1016/j.neurobiolaging.2014.10.004

Klemm, F., and J.A. Joyce. 2015. Microenvironmental regulation of therapeutic response in cancer. *Trends Cell Biol.* 25:198–213. https://doi.org/10.1016/j.tcb.2014.11.006

Kodack, D.P., V. Askoxylakis, G.B. Ferraro, Q. Sheng, M. Badeaux, S. Goel, X. Qi, R. Shankaraiah, Z.A. Cao, R.R. Ramjiawan, et al. 2017. The brain microenvironment mediates resistance in luminal breast cancer to PI3K inhibition through HER3 activation. *Sci. Transl. Med.* 9:eaal4682. https://doi.org/10.1126/scitranslmed.aal4682

Kouhara, H., Y.R. Hadari, T. Spivak-Kroizman, J. Schilling, D. Bar-Sagi, I. Lax, and J. Schlessinger. 1997. A lipid-anchored Grb2-binding protein that links FGF-receptor activation to the Ras/MAPK signaling pathway. *Cell.* 89:693–702. https://doi.org/10.1016/S0092-8674(00)80252-4

Krop, I.E., I.A. Mayer, V. Ganju, M. Dickler, S. Johnston, S. Morales, D.A. Yardley, B. Melichar, A. Forero-Torres, S.C. Lee, et al. 2016. Pictilisib for oestrogen receptor-positive, aromatase inhibitor-resistant, advanced or metastatic breast cancer (FERGI): a randomised, double-blind, placebo-controlled, phase 2 trial. *Lancet Oncol.* 17:811–821. https://doi.org/10.1016/S1470-2045(16)00106-6

Larsen, S.S., M. Egeblad, M. Jäättelä, and A.E. Lykkesfeldt. 1999. Acquired antiestrogen resistance in MCF-7 human breast cancer sublines is not accomplished by altered expression of receptors in the ErbB-family. *Breast Cancer Res. Treat.* 58:41–56. https://doi.org/10.1023/A:1006232830161

Linder, C., P. Byström, G. Engel, G. Auer, U. Aspenblad, H. Strander, and S. Linder. 1998. Correlation between basic fibroblast growth factor immunostaining of stromal cells and stromelysin-3 mRNA expression in human breast carcinoma. *Br. J. Cancer.* 77:941–945. https://doi.org/10.1038/bjc.1998.155

Loi, S., B. Haibe-Kains, C. Desmedt, P. Wirapati, F. Lallemand, A.M. Tutt, C. Gillet, P. Ellis, K. Ryder, J.F. Reid, et al. 2008. Predicting prognosis using molecular profiling in estrogen receptor-positive breast cancer treated with tamoxifen. *BMC Genomics.* 9:239. https://doi.org/10.1186/1471-2164-9-239

Ma, C.X., T. Reinert, I. Chmielewska, and M.J. Ellis. 2015. Mechanisms of aromatase inhibitor resistance. *Nat. Rev. Cancer.* 15:261–275. https://doi.org/10.1038/nrc3920

Miller, T.W., J.M. Balko, and C.L. Arteaga. 2011. Phosphatidylinositol 3-kinase and antiestrogen resistance in breast cancer. *J. Clin. Oncol.* 29:4452–4461. https://doi.org/10.1200/JCO.2010.34.4879

Musolino, A., M. Campone, P. Neven, N. Denduluri, C.H. Barrios, J. Cortes, K. Blackwell, H. Soliman, Z. Kahan, H. Bonnefoi, et al. 2017. Phase II, randomized, placebo-controlled study of dovitinib in combination with fulvestrant in postmenopausal patients with HR+, HER2- breast cancer

that had progressed during or after prior endocrine therapy. *Breast Cancer Res.* 19:18. https://doi.org/10.1186/s13058-017-0807-8

Owens, P., E. Engelking, G. Han, S.M. Haeger, and X.J. Wang. 2010. Epidermal Smad4 deletion results in aberrant wound healing. *Am. J. Pathol.* 176:122–133. https://doi.org/10.2353/ajpath.2010.090081

Petrone, A., M.E. Adamo, C. Cheng, and A.N. Kettenbach. 2016. Identification of Candidate Cyclin-dependent kinase 1 (Cdk1) Substrates in Mitosis by Quantitative Phosphoproteomics. *Mol. Cell. Proteomics.* 15:2448–2461. https://doi.org/10.1074/mcp.M116.059394

Quail, D.F., and J.A. Joyce. 2013. Microenvironmental regulation of tumor progression and metastasis. *Nat. Med.* 19:1423–1437. https://doi.org/10.1038/nm.3394

Reis-Filho, J.S., P.T. Simpson, N.C. Turner, M.B. Lambros, C. Jones, A. Mackay, A. Grigoriadis, D. Sarrio, K. Savage, T. Dexter, et al. 2006. FGFR1 emerges as a potential therapeutic target for lobular breast carcinomas. *Clin. Cancer Res.* 12:6652–6662. https://doi.org/10.1158/1078-0432.CCR-06-1164

Robinson, M.D., and A. Oshlack. 2010. A scaling normalization method for differential expression analysis of RNA-seq data. *Genome Biol.* 11:R25. https://doi.org/10.1186/gb-2010-11-3-r25

Rudas, M., M. Lehnert, A. Huynh, R. Jakesz, C. Singer, S. Lax, W. Schippinger, O. Dietze, R. Greil, W. Stiglbauer, et al. Austrian Breast and Colorectal Cancer Study Group. 2008. Cyclin D1 expression in breast cancer patients receiving adjuvant tamoxifen-based therapy. *Clin. Cancer Res.* 14:1767–1774. https://doi.org/10.1158/1078-0432.CCR-07-4122

Seghezzi, G., S. Patel, C.J. Ren, A. Gualandris, G. Pintucci, E.S. Robbins, R.L. Shapiro, A.C. Galloway, D.B. Rifkin, and P. Mignatti. 1998. Fibroblast growth factor-2 (FGF-2) induces vascular endothelial growth factor (VEGF) expression in the endothelial cells of forming capillaries: an autocrine mechanism contributing to angiogenesis. *J. Cell Biol.* 141:1659–1673. https://doi.org/10.1083/jcb.141.7.1659

Siegel, R., C. DeSantis, K. Virgo, K. Stein, A. Mariotto, T. Smith, D. Cooper, T. Gansler, C. Lerro, S. Fedewa, et al. 2012. Cancer treatment and survivorship statistics, 2012. *CA Cancer J. Clin.* 62:220–241. https://doi.org/10.3322/caac.21149

Smith, K., S.B. Fox, R. Whitehouse, M. Taylor, M. Greenall, J. Clarke, and A.L. Harris. 1999. Upregulation of basic fibroblast growth factor in breast carcinoma and its relationship to vascular density, oestrogen receptor, epidermal growth factor receptor and survival. *Ann. Oncol.* 10:707–713. https://doi.org/10.1023/A:1008303614441

Straussman, R., T. Morikawa, K. Shee, M. Barzily-Rokni, Z.R. Qian, J. Du, A. Davis, M.M. Mongare, J. Gould, D.T. Frederick, et al. 2012. Tumour micro-environment elicits innate resistance to RAF inhibitors through HGF secretion. *Nature.* 487:500–504. https://doi.org/10.1038/nature11183

Subramanian, A., P. Tamayo, V.K. Mootha, S. Mukherjee, B.L. Ebert, M.A. Gillette, A. Paulovich, S.L. Pomeroy, T.R. Golub, E.S. Lander, and J.P. Mesirov. 2005. Gene set enrichment analysis: a knowledge-based approach for interpreting genome-wide expression profiles. *Proc. Natl. Acad. Sci. USA.* 102:15545–15550. https://doi.org/10.1073/pnas.0506580102

Symmans, W.F., C. Hatzis, C. Sotiriou, F. Andre, F. Peintinger, P. Regitnig, G. Daxenbichler, C. Desmedt, J. Domont, C. Marth, et al. 2010. Genomic index of sensitivity to endocrine therapy for breast cancer. *J. Clin. Oncol.* 28:4111–4119. https://doi.org/10.1200/JCO.2010.28.4273

Teicher, B.A., T.S. Herman, S.A. Holden, Y.Y. Wang, M.R. Pfeffer, J.W. Crawford, and E. Frei III. 1990. Tumor resistance to alkylating agents conferred by mechanisms operative only in vivo. *Science.* 247:1457–1461. https://doi.org/10.1126/science.2108497

Tivari, S., R. Korah, M. Lindy, and R. Wieder. 2015. An In Vitro Dormancy Model of Estrogen-sensitive Breast Cancer in the Bone Marrow: A Tool for Molecular Mechanism Studies and Hypothesis Generation. *J. Vis. Exp.* 100:e52672.

Turner, N., A. Pearson, R. Sharpe, M. Lambros, F. Geyer, M.A. Lopez-Garcia, R. Natrajan, C. Marchio, E. Iorns, A. Mackay, et al. 2010. FGFR1 amplification drives endocrine therapy resistance and is a therapeutic target in breast cancer. *Cancer Res.* 70:2085–2094. https://doi.org/10.1158/0008-5472.CAN-09-3746

Turner, N.C., J. Ro, F. André, S. Loi, S. Verma, H. Iwata, N. Harbeck, S. Loibl, C. Huang Bartlett, K. Zhang, et al. PALOMA3 Study Group. 2015. Palbociclib in Hormone-Receptor-Positive Advanced Breast Cancer. *N. Engl. J. Med.* 373:209–219. https://doi.org/10.1056/NEJMoa1505270

Uhlén, M., L. Fagerberg, B.M. Hallström, C. Lindskog, P. Oksvold, A. Mardinoglu, Å. Sivertsson, C. Kampf, E. Sjöstedt, A. Asplund, et al. 2015. Proteomics. Tissue-based map of the human proteome. *Science.* 347:1260419. https://doi.org/10.1126/science.1260419

Vaillant, F., D. Merino, L. Lee, K. Breslin, B. Pal, M.E. Ritchie, G.K. Smyth, M. Christie, L.J. Phillipson, C.J. Burns, et al. 2013. Targeting BCL-2 with the BH3 mimetic ABT-199 in estrogen receptor-positive breast cancer. *Cancer Cell.* 24:120–129. https://doi.org/10.1016/j.ccr.2013.06.002

van de Vijver, M.J., Y.D. He, L.J. van't Veer, H. Dai, A.A. Hart, D.W. Voskuil, G.J. Schreiber, J.L. Peterse, C. Roberts, M.J. Marton, et al. 2002. A gene-expression signature as a predictor of survival in breast cancer. *N. Engl. J. Med.* 347:1999–2009. https://doi.org/10.1056/NEJMoa021967

Varn, F.S., M.H. Ung, S.K. Lou, and C. Cheng. 2015. Integrative analysis of survival-associated gene sets in breast cancer. *BMC Med. Genomics.* 8:11. https://doi.org/10.1186/s12920-015-0086-0

Wang, L., H. Park, S. Chhim, Y. Ding, W. Jiang, C. Queen, and K.J. Kim. 2012a. A novel monoclonal antibody to fibroblast growth factor 2 effectively inhibits growth of hepatocellular carcinoma xenografts. *Mol. Cancer Ther.* 11:864–872. https://doi.org/10.1158/1535-7163.MCT-11-0813

Wang, T., A.N. Kettenbach, S.A. Gerber, and C. Bailey-Kellogg. 2012b. MMFPh: a maximal motif finder for phosphoproteomics datasets. *Bioinformatics.* 28:1562–1570. https://doi.org/10.1093/bioinformatics/bts195

Wilcken, N.R., O.W. Prall, E.A. Musgrove, and R.L. Sutherland. 1997. Inducible overexpression of cyclin D1 in breast cancer cells reverses the growth-inhibitory effects of antiestrogens. *Clin. Cancer Res.* 3:849–854.

Wilson, T.R., J. Fridlyand, Y. Yan, E. Penuel, L. Burton, E. Chan, J. Peng, E. Lin, Y. Wang, J. Sosman, et al. 2012. Widespread potential for growth-factor-driven resistance to anticancer kinase inhibitors. *Nature.* 487:505–509. https://doi.org/10.1038/nature11249

Xing, Y., T. Yu, Y.N. Wu, M. Roy, J. Kim, and C. Lee. 2006. An expectation-maximization algorithm for probabilistic reconstructions of full-length isoforms from splice graphs. *Nucleic Acids Res.* 34:3150–3160. https://doi.org/10.1093/nar/gkl396

Yu, Q., Y. Geng, and P. Sicinski. 2001. Specific protection against breast cancers by cyclin D1 ablation. *Nature.* 411:1017–1021. https://doi.org/10.1038/35082500

Yu, Q., E. Sicinska, Y. Geng, M. Ahnström, A. Zagozdzon, Y. Kong, H. Gardner, H. Kiyokawa, L.N. Harris, O. Stål, and P. Sicinski. 2006. Requirement for CDK4 kinase function in breast cancer. *Cancer Cell.* 9:23–32. https://doi.org/10.1016/j.ccr.2005.12.012